



Nanoporous hematite nanoparticles: Synthesis and applications for benzylation of benzene and aromatic compounds



Nguyen Duc Cuong^{a,b,c}, Nguyen Duc Hoa^{a,*}, Tran Thai Hoa^c, Dinh Quang Khieu^c, Duong Tuan Quang^d, Vu Van Quang^a, Nguyen Van Hieu^{a,*}

^a International Training Institute for Materials Science (ITIMS), Hanoi University of Science and Technology, No. 1, Dai Co Viet, Hanoi, Viet Nam

^b Faculty of Hospitality and Tourism, Hue University, 22 Lam Hoang, Hue City, Viet Nam

^c College of Sciences, Hue University, 77 Nguyen Hue, Hue City, Viet Nam

^d College of Education, Hue University, 34 Le Loi, Hue City, Viet Nam

ARTICLE INFO

Article history:

Received 12 July 2013

Received in revised form 7 August 2013

Accepted 7 August 2013

Available online 16 August 2013

Keywords:

α -Fe₂O₃

Nanoporous

Benzylation

Diphenylmethane

ABSTRACT

The catalytic benzylation of benzene and other aromatic compounds is one of the most important reactions in the synthesis of pharmaceutical compounds. In this study, we report the synthesis of nanoporous α -Fe₂O₃ nanoparticles via a hydrothermal method and their application in the catalytic benzylation of benzene and benzyl chloride in the fabrication of diphenylmethane. Crystal structure and morphology characterization results demonstrated that the hydrothermal method enabled the fabrication of highly dispersed α -Fe₂O₃ nanoparticles with spherical shape and an average size of 100 nm. The α -Fe₂O₃ nanoparticles have nanopores of less than 10 nm that are randomly distributed inside the nanoparticles. The catalytic benzylation of benzene and benzyl chloride was conducted over the synthesized α -Fe₂O₃ nanoparticles. The results demonstrated that the synthesized α -Fe₂O₃ nanoparticles are effective catalysts for the benzylation of benzene and benzyl chloride with high activity and selectivity.

© 2013 Elsevier B.V. All rights reserved.

1. Introduction

Catalytic Friedel–Crafts alkylations are a very important class of reactions that are commonly used in organic chemistry to synthesize various pharmaceutical compounds [1,2]. One of the most important products synthesized via the Friedel–Crafts reaction between benzene and benzyl chloride is diphenylmethane (DPM), which is commonly used in the fragrance industry as (i) both fixative and scented agent or (ii) as monomers for the synthesis of polycarbonate resins [3–5]. Friedel–Crafts alkylations, however, require a strong Lewis acid catalyst.

Among the catalysts, transition metal oxides, such as iron oxides, have been immensely popular in a wide range of applications because of their ease in handling, relatively low cost, nontoxicity, and environment-friendly property. Iron oxide catalysts are currently utilized on a large scale basis in laboratory, industrial, and environmental processes [1–8]. Hematite (α -Fe₂O₃) is one of the most stable forms of iron oxides, which has been widely used as a catalyst in numerous reactions, such as the decomposition of soot

and NO_x in diesel exhausts [9–11], photocatalytic degradation of salicylic acid [12], thermal decomposition of ammonium perchlorate [13], oxidation of CO [14], decomposition of biomass tars [15], cracking of catechols and hydroquinones [16], and Fischer–Tropsch synthesis [17]. An iron-based solid catalyst is also normally used as a Lewis acid catalyst and/or support in homogeneous and heterogeneous catalysis [18–20].

The catalytic activity of transition metal oxides is strongly dependent on their morphology and specific surface area. A porous structure with a relatively large surface area is expected to have a good catalytic performance. Fe-based solid catalysts, such as Fe–TUD-1 [21], Fe–ZSM-5 [22], Fe–M–Mor [23], Fe–Al₂O₃ [24], Fe–SBA [25], and Fe–MCM-41 [26,27], have been widely used for the benzylation of benzene with benzyl chloride (BC). However, findings on the active sites for the reaction [28] and the reaction induction period are still debatable. Choudhary et al. [29] hypothesized that the reducible Fe species were relative to the reactivity of Fe–HZSM-5. Sun et al. [30] reported that the highly dispersed iron oxide nanoclusters on Fe–SBA-15 were active sites for the reaction. Arafat and Alhamed [31] considered that the high redox potential Fe³⁺ incorporated in the MCM-41 silica matrix and Fe₂O₃ caused the high reactivity of Fe–CMC-41. With regards to the reaction induction period, Choudhary et al. [27,29] hypothesized that the reaction induction period was caused by the presence of moisture in the reaction mixture and that the catalysts

* Corresponding authors. Address: International Training Institute for Materials Science (ITIMS), Hanoi University of Science and Technology (HUST), No. 1, Dai Co Viet Road, Hanoi, Viet Nam. Tel.: +84 4 38680787; fax: +84 4 38692963.

E-mail addresses: ndhoa@itims.edu.vn (N.D. Hoa), hieu@itims.edu.vn (N.V. Hieu).

are activated during the initial reaction period. Leng et al. [23] suggested that the reaction induction period seemed to depend on the catalytic activity. A high activity indicates a short induction period. However, the function of iron oxides in active catalysts remains unclear. In addition, the benzylation of benzene with BC over nanoporous α -Fe₂O₃ nanoparticles has not yet been explored. Thereby, further study is needed to explicitly understand the catalytic performance of nanoporous α -Fe₂O₃ nanoparticles for benzylation of benzene with BC.

In this article, we report the controlled synthesis of scalable nanoporous α -Fe₂O₃ nanoparticles for benzene benzylation. The nanoporous α -Fe₂O₃ nanoparticles were synthesized via a hydrothermal method, and their catalytic performances in the benzylation of benzene and other aromatics with BC were systematically investigated. The results showed that the nanoporous hematite nanoparticles are active and selective catalysts for the benzylation of benzene with BC to yield DPM.

2. Experimental

2.1. Materials

Urea, Fe(NO₃)₃·9H₂O, benzene, benzyl chloride, toluene, and *p*-xylene were purchased from Merck. Cetyltrimethylammonium bromide (CTAB) was purchased from Aldrich. All chemicals were used as received without further purification.

2.2. Synthesis of nanoporous α -Fe₂O₃ nanoparticles

Nanoporous α -Fe₂O₃ nanoparticles were synthesized via a hydrothermal method by using urea and iron(III) nitrate nonahydrate as precursors and CTAB as a surfactant. Ferric nitrate (2 mmol), CTAB (1 g), and urea (15 mmol) were dissolved in 35 mL of distilled water via magnetic stirring at room temperature for 2 h to obtain a slurry solution. The slurry solution was then transferred into a 100 mL Teflon-lined autoclave for hydrothermal processing. The hydrothermal processing was carried out at 80 °C for 36 h, and the solution was then cooled down to room temperature. The products were collected by several cycles of centrifugation and washed with distilled water and ethanol. The collected products were dried at 60 °C for 24 h and then heat-treated at 500 °C to remove organic residues.

2.3. Material characterization

The crystal structure of the nanoporous α -Fe₂O₃ nanoparticles was characterized using an X-ray diffractometer (XRD, D8 Advance, Bruker, Germany) with Cu K α ($\lambda = 1.54$ nm) radiation. Infrared spectroscopy was performed to evaluate the surface state of the synthesized materials. The infrared spectra were obtained using a Nicolet 6700 FTIR Spectrometer in the range of 400–4700 cm⁻¹ with a spectral resolution of 4 cm⁻¹ in transmittance mode. The KBr pellet technique was used for sampling with 1 wt.% of materials for infrared spectroscopy measurement. The morphology and the average particle size of hematite nanoparticles were investigated via scanning electron microscopy (SEM, Model JSM-5300LV) and transmission electron microscopy (TEM, Model JEOL-3432, Japan). The nitrogen adsorption/desorption isotherms of the heat-treated samples were obtained using a Micromeritics at 77 K. The specific surface area of the sample was calculated using the Brunauer–Emmett–Teller (BET) method, whereas the pore-size distribution was determined from the desorption isotherm data by using the Barrett–Joyner–Halenda (BJH) model.

2.4. Friedel–Crafts type benzylation of benzene

A scheme that represents the proposed mechanism for the benzylation of benzene over the nanoporous α -Fe₂O₃ nanoparticles catalysts is shown in Fig. 1 [22,26]. The liquid phase Friedel–Crafts benzylation reactions over α -Fe₂O₃ nanoparticle catalysts were carried out in a mechanically stirred mode in a two-neck round-bottomed flask (capacity: 100 mL), which was fitted with a reflux condenser and heated in a precisely controlled oil bath. All the reactions were performed in air atmosphere. Benzene (30.55 g, 391 mmol), benzyl chloride (1.1 g, 8.7 mmol), and hematite catalyst (50 mg) were mixed and stirred at 358 K at a moderate speed for at least 3 min. The liquid samples were extracted, filtered periodically, and analyzed via gas chromatography (GC-2010 Shimadzu series) equipped with a thermal conductivity detector (TCD) to evaluate the catalytic activity. The catalytic conversion was calculated from the amount of benzyl chloride that was consumed during the reaction, and the products were confirmed via GC–MS. Details about the GC–MS results can be found in the electronic supporting information (ESI).

3. Results and discussion

3.1. Characterization of catalyst

The crystal structure of the as-prepared α -Fe₂O₃ nanoparticles were examined via powder XRD measurement, and the data is shown in Fig. 2. The observed pattern of the collected products exhibited all the expected peaks from the α -Fe₂O₃ structure without any detectable peak from impurities and other phases. The diffraction peaks were well-indexed to the rhombohedral structure of α -Fe₂O₃ [space group: R3c] with structural parameters of $a = b = 0.0356$ Å, $c = 13.7489$ Å, $\alpha = \beta = 90^\circ$, and $\gamma = 120^\circ$, which agree with the literature (JCPDS 33-0664). The average crystalline size of the α -Fe₂O₃ nanoparticles calculated from the XRD data by using the Scherrer equation is about 35 nm.

The surface state of the synthesized α -Fe₂O₃ nanoparticles investigated via FTIR is shown in Fig. 3. The absorption peaks at 474 and 544 cm⁻¹ are original peaks from α -Fe₂O₃ nanoparticles [32], whereas the peaks at 1634 cm⁻¹ and 3436 cm⁻¹ are due to the OH bending of water and the hydroxyl group (–OH), respectively [33].

The morphologies of the nanoporous α -Fe₂O₃ nanoparticles, which were characterized from SEM and TEM images, are shown in Fig. 4(A and B), respectively. The α -Fe₂O₃ nanoparticles fabricated via hydrothermal synthesis have very homogenous morphologies with nearly spherical shapes and regular dispersion (Fig. 4(A)). The average particle size of the nanoparticles is about 100 nm, which is larger than the average crystalline size estimated from the Scherrer equation (35 nm). This result suggests that the nanoparticle is not a single crystal but is a poly-crystal. The TEM image also indicates that nanopores of about less than 10 nm are randomly distributed inside the α -Fe₂O₃ nanoparticles (Fig. 4(B)). These nanopores are believed to be generated because of the presence of bubbles during the hydrothermal process. The water expulsion of iron oxyhydroxide via heat treatment at 500 °C may also contribute to the formation of the nanopores. However, the XRD pattern of as-hydrothermal α -Fe₂O₃ samples (Fig. S1) shows typical diffraction peaks of an α -Fe₂O₃ phase but not of iron oxyhydroxide. Therefore, the possibility of the formation of the nanopores as a result of water expulsion could be eliminated.

Fig. 5 shows the N₂ adsorption/desorption isotherms and pore size distributions of the α -Fe₂O₃ nanoparticles. The sample exhibits a type IV N₂ adsorption/desorption isotherm with the H1 hysteresis loop (Fig. 5), which indicates the presence of mesoporosity within the nanoparticles [34]. The pore diameters (inset of Fig. 5) calculated using the BJH method are about 81 nm, and the pores are caused by the interparticle space that is formed by the aggregation of Fe₂O₃ nanocrystals upon calcination. The BET specific surface area of the nanoporous α -Fe₂O₃ nanoparticles is 15 m²/g. This value is relatively high considering the size of the nanoparticles. The catalytic activity greatly depends on the morphologies and specific surface area of the catalysts because they have different fractions of atoms located at different corners and edges as well as different defects that are caused by the loss of atoms at these locations.

3.2. Benzylation of benzene and other aromatic compounds

To evaluate the catalytic performance of the nanoporous α -Fe₂O₃ nanoparticles, the benzylation of benzene with BC was investigated. The reaction was carried out at 358 K and 50 mg of the catalyst was used. Fig. 6 shows the conversion of BC and product distribution as a function of reaction time. The BC conversion reached 100% in a very fast reaction time of about 3 min. The reaction induction period depends on the catalytic activity [23], but the

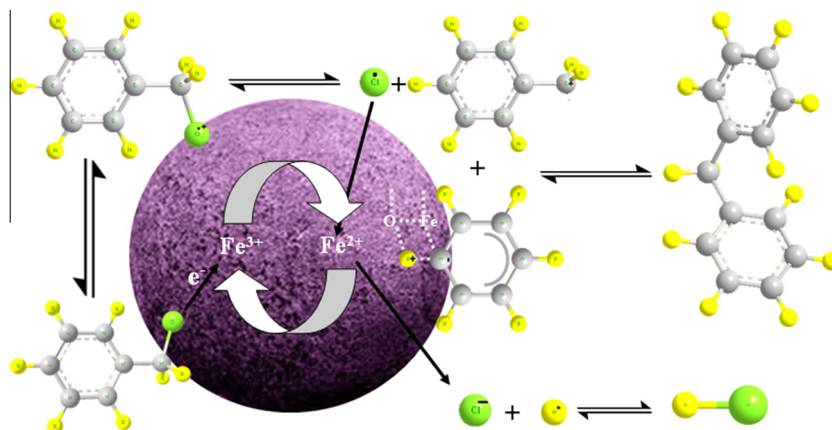


Fig. 1. Scheme depicting the proposed mechanism for the benzylation of benzene over the nanoporous α -Fe₂O₃ nanoparticles as catalyst.

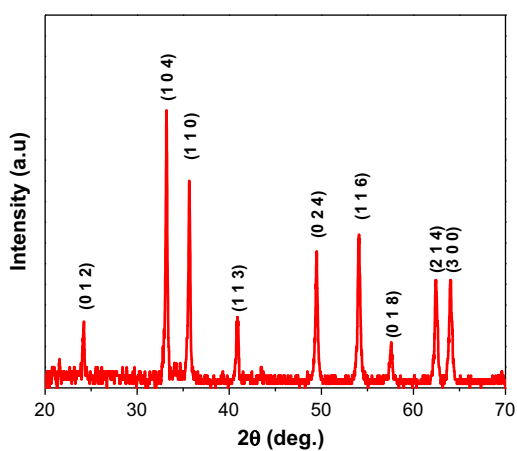


Fig. 2. XRD pattern of the α -Fe₂O₃ nanoparticles fabricated via the hydrothermal method.

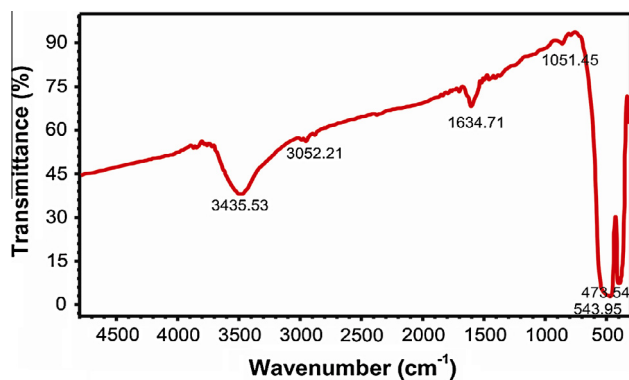


Fig. 3. FTIR spectra of the α -Fe₂O₃ nanoparticles.

α -Fe₂O₃ nanoparticles in the current study had a very high activity with almost no reaction induction period. A high activity indicates a short induction period. Comparing the catalytic activity of the nanoporous α -Fe₂O₃ nanoparticles with those of other Fe-solid based catalysts, such as Fe-SBA-15 [1], FeKIT-5 [5], Fe-M-Mor [23], Fe-Al₂O₃ [24], Fe/Si-MCM-41 [27], and Fe₂O₃/HZM-5 [35], the nanoporous α -Fe₂O₃ nanoparticles are more active. In general, the catalytic activity depends on the iron content in the catalyst, which comes into contact with the benzylation agents. The catalyst

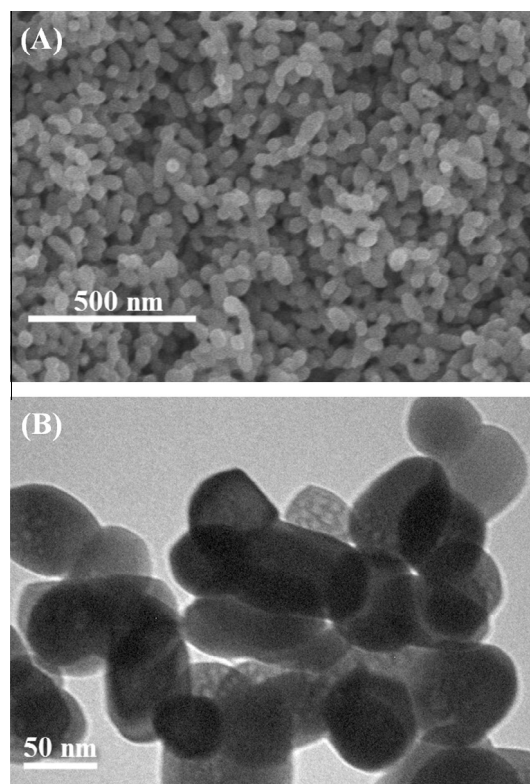


Fig. 4. (A) SEM and (B) TEM images of the nanoporous Fe₂O₃ nanoparticles.

with the highest iron content showed the highest catalytic activity [5,21,23,35]. In addition, the high catalyst activity of the Fe-solid catalyst is usually caused by its porous structure and the presence of iron oxide. For instance, Anand et al. [5] studied the benzylation of benzene over FeKIT-5 (12), which contains a lot of iron species. The higher catalytic activity of FeKIT-5 (12) was attributed to its three-dimensional cage-type porous structure and high iron content. Hamdy et al. [21] demonstrated that the nanoparticles of iron oxide were less coordinately saturated (because of lattice strain and defects) than isolated iron species or the iron centers present in larger particles, thereby giving rise to more active sites. Leng et al. reported that the presence of more iron oxide nanoclusters could contribute to the improvement of catalytic activity [23]. In the present study, the higher catalytic activity of α -Fe₂O₃ nanoparticles was possibly due to its high iron content and porous

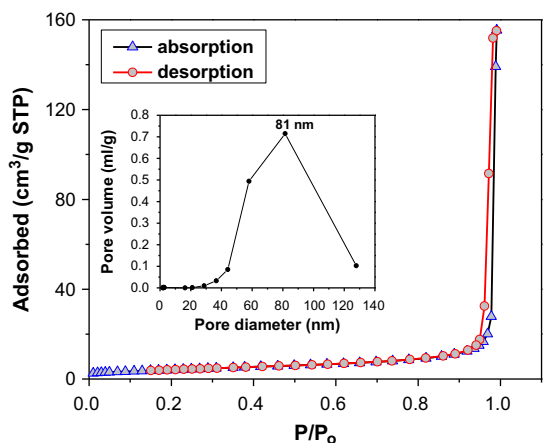


Fig. 5. Nitrogen adsorption/desorption isotherms and BJH pore size distribution (inset) of the nanoporous α -Fe₂O₃ nanoparticles.

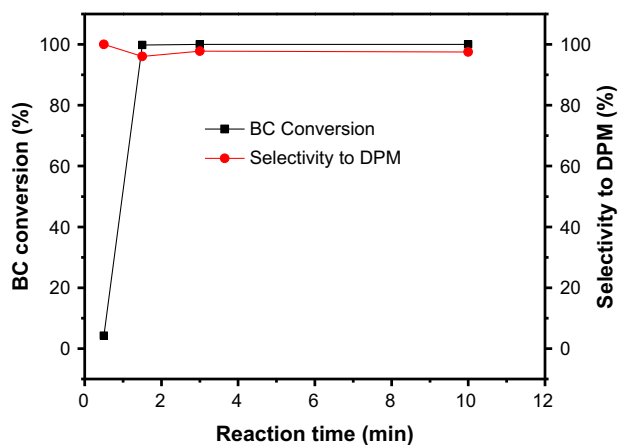


Fig. 6. Percentage conversion and selectivity versus time for the reaction between benzene and BC at 358 K (molar ratio benzene/BC of 45:1, 50 mg of α -Fe₂O₃ as a catalyst).

structure, which provided larger active sites. Moreover, the difference in the catalytic activity of the α -Fe₂O₃ nanoparticles could possibly be attributed to the existence of mesopores that greatly overcame the diffusion limitation compared with microporous catalysts.

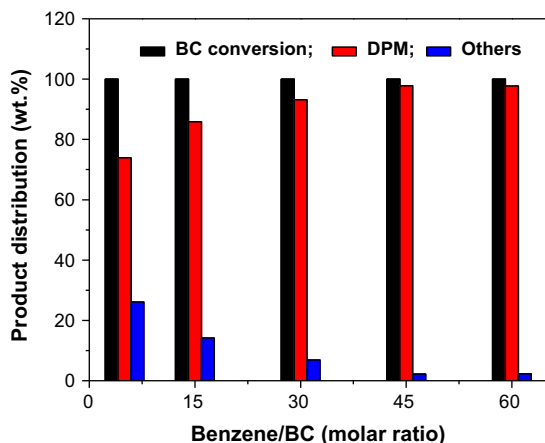


Fig. 7. Influence of benzene/BC molar ratio on the conversion of BC and product distribution (Reaction condition: 358 K, 50 mg of α -Fe₂O₃).

Table 1

Benylation of benzene with benzyl chloride at different catalyst mass.

Catalyst (mg)	Time (min)	BC conversion (%)	DPM selectivity
10	3	5.23	100
50	3	100	97.76
100	3	100	95.33
500	3	100	89.93

Conditions: benzene = 391.1 mmol, benzyl chloride = 8.7 mmol, time = 3 min, temperature = 358 K.

Table 2

Catalytic activities of the nanoporous α -Fe₂O₃ nanoparticles at different temperatures.

Temperature (K)	Time (min)	BC conversion (%)	DPM selectivity
343	60	3.5	100.00
358	3	100	97.76
373	3	100	95.24
393	3	100	85.86

Condition: benzene = 391.1 mmol, benzyl chloride = 8.7 mmol, catalyst = 50 mg.

Table 3

Influence of different electron donating substitution groups for the benzene benzylation reaction over α -Fe₂O₃ nanoparticles.

Aromatic substances	Reaction time (min)	Reaction temperature (K)	BC conversion	Reaction product(s) (selectivity %)
Benzene	3	358	100	Diphenylmethane (97.76%)
Toluene	3	368	100	0-Benzyltoluene (52.36%) <i>p</i> -benzyltoluene (47.64%)
<i>p</i> -Xylene	3	378	100	2-Benzyl-1,3-dimethylbenzene (99.93%)

The influence of the stoichiometric ratio between benzene and BC for the benzylation reaction was also studied, and the data is shown in Fig. 7. The benzylation of benzene was carried out at 358 K for 3 min with various molar ratios of benzene/BC by using 50 mg of the catalyst. The benzene/BC ratio was changed by keeping the amount of BC constant while varying the amount of benzene. The result shows that the ratio between benzene and BC appears to have a strong influence on the selectivity to DPM (Fig. 7). The conversion of BC reached to 100% in all the ratios. The selectivity towards DPM is increased with increasing benzene content. At a ratio benzene/BC of 45, a selectivity of approximately 100% can be achieved. The increase in DPM selectivity with increasing benzene/BC ratio can be attributed to enhancement of benzene over the catalyst surface and a higher dilution of BC.

The reaction profile when different amounts of nanoporous α -Fe₂O₃ nanoparticle catalysts were used reveals that selectivity to DPM is higher at a lower concentration (Table 1). At a higher α -Fe₂O₃ concentration, the conversion of BC increases to an optimum value and the formation rate of other products also increases. Hence, an optimum amount of 50 mg of catalyst in the reaction mixture is ideal for achieving better conversion (100%) and selectivity for DPM (97.76%).

The effect of temperature on the benzylation activity of α -Fe₂O₃ nanoparticles was also investigated, and the results are shown in Table 2. The performance of the catalysts strongly increases with increasing reaction temperature. At a reaction temperature of 343 K and a reaction time of 1 h, the conversion of BC and the

selectivity to DPM are 3.5% and 100%, respectively. When the reaction temperature was increased to 358 K, the BC conversion increases from 3.5% to 100%, but the selectivity to DPM decreases from 100% to 97.76% for a reaction time of 3 min. The selectivity to DPM is only 85.86% at 393 K. These results reveal that the conversion of BC and the selectivity towards DPM can be easily tuned by simply adjusting the reaction temperature.

The benzylation reaction over α -Fe₂O₃ nanoparticles was also investigated for other aromatic compounds, such as toluene and *p*-xylene, to check the effluence of substitution groups attached to the aromatic ring on the BC conversion and selectivity of products. As shown in Table 3, the reaction temperatures for 100% conversion of BC within 3 min increase in the following order: benzene < toluene < *p*-xylene. According to the classical mechanism of the Friedel–Crafts-type acid-catalyzed benzylation reaction, the benzylation of an aromatic compound is easier if one or more electron-donating groups are present in the aromatic ring [27], and the rate of benzylation for the aromatic compound is expected to follow have a trend as follows: *p*-xylene > toluene > benzene. However, the observation in the present case is opposite to the classical mechanism, and it is in agreement with the previously proposed redox mechanism of the Friedel–Crafts type Fe-solid [25,27].

4. Conclusions

We introduced the synthesis and application of nanoporous α -Fe₂O₃ nanoparticles and investigated their catalytic performances for the benzylation of benzene and several aromatic compounds. Well-dispersed nanoporous α -Fe₂O₃ nanoparticles with an average size of 100 nm, which had nanopores of less than 10 nm, were prepared via a hydrothermal method. The α -Fe₂O₃ nanoparticles showed excellent catalytic performance in the benzylation of benzene with benzyl chloride, which leads to the formation of DPM with high selectivity. The BC conversion reached 100% in a reaction time of 3 min with 97.76% selectivity to DPM. The conversion and product distribution are largely dependent on the experimental conditions. The selectivity of DPM increases with increasing benzene/BC molar ratio but decreases with increasing catalyst amount and reaction temperature. The nanoporous α -Fe₂O₃ nanoparticles also had potential applications in other Friedel–Crafts alkylations, especially in large molecular reactions.

Acknowledgment

This work was financially supported by the Vietnam's National Foundation for Science and Technology Development (Nafosted, Code: 104.03-2012.54)

Appendix A. Supplementary material

Supplementary data associated with this article can be found, in the online version, at <http://dx.doi.org/10.1016/j.jallcom.2013.08.057>.

References

- [1] K. Bachari, O. Cherifi, Catal. Commun. 7 (2006) 926–930.
- [2] A.E. Ahmed, F. Adam, Micropor. Mesopor. Mat. 118 (2009) 35–43.
- [3] C. Anand, B. Sathyaseelan, L. Samie, A. Beitollahi, R. Pradeep Kumar, M. Palanichamy, V. Murugesan, El-Refaie Kenawy, Salem S. Al-Deyab, A. Vinu, Micropor. Mesopor. Mat. 134 (2010) 87–92.
- [4] V.D. Chaube, Catal. Commun. 5 (2004) 321–326.
- [5] C. Anand, S.V. Priya, G. Lawrence, D.S. Dhawale, S. Varghese, M.A. Wahab, K.S. Prasad, A. Vinu, Catal. Today 204 (2013) 125–131.
- [6] M. Hermanek, R. Zboril, I. Medrik, J. Pechousek, C. Gregor, J. Am. Chem. Soc. 129 (2007) 10929–10936.
- [7] F. Shi, M.K. Tsea, M.M. Pohl, J. Radnik, A. Brückner, S. Zhang, M. Bellera, J. Mol. Catal. A: Chem. 292 (2008) 28–35.
- [8] H. Liu, Y. Wei, P. Li, Y. Zhang, Y. Sun, Mater. Chem. Phys. 102 (2007) 1–6.
- [9] D. Reichert, T. Finke, N. Atanassova, H. Bockhorn, S. Kureti, Appl. Catal. B: Environ. 84 (2008) 803–812.
- [10] D. Reichert, H. Bockhorn, S. Kureti, Catal. B: Environ. 80 (2008) 248–259.
- [11] S. Wagloehner, S. Kureti, Appl. Catal. B: Environ. 125 (2012) 158–165.
- [12] J. Gu, S. Li, E. Wang, Q. Li, G. Sun, R. Xu, H. Zhang, J. Solid State Chem. 182 (2009) 1265–1272.
- [13] H. Xu, X. Wang, L. Zhang, Powder Technol. 185 (2008) 176–180.
- [14] M.H. Khedr, K.S. Abdel Halim, M.I. Nasr, A.M. El-Mansy, Mat. Sci., Eng. A 430 (2006) 40–45.
- [15] M.A. Uddin, H. Tsuda, S. Wu1, E. Sasaoka, Fuel 87 (2008) 451–459.
- [16] E.J. Shin, D.E. Miser, W.G. Chan, M.R. Hajaligol, Appl. Catal. B: Environ. 61 (2005) 79–89.
- [17] D. Mahajan, P. Gütlich, U. Stumm, Catal. Commun. 4 (2003) 101–107.
- [18] C. Bolm, J. Legros, J.L. Paih, L. Zani, Chem. Rev. 104 (2004) 6217–6254.
- [19] M. Costas, K. Chen, Q. Lawrence Jr., Coord. Chem. Rev. 200–202 (2000) 517–544.
- [20] B. Moens, H.D. Winne, S. Corthals, H. Poelman, R.D. Gryse, V. Meynen, P. Cool, B.F. Sels, P.A. Jacobs, J. Catal. 247 (2007) 86–100.
- [21] M.S. Hamdy, G. Mul, J.C. Jansen, A. Ebaid, Z. Shan, A.R. Overweg, Th. Maschmeyer, Catal. Today 100 (2005) 255–260.
- [22] E. Díaz, S. Ordóñez, A. Vega, A. Auroux, J. Coca, Appl. Catal. A: Gen. 295 (2005) 106–115.
- [23] K. Leng, S. Sun, B. Wang, L. Sun, W. Xu, Y. Sun, Catal. Commun. 28 (2012) 64–68.
- [24] M.S. Niasari, J. Hasanalian, H. Najafian, J. Mol. Catal. A: Chem. 209 (2004) 209–214.
- [25] K. Bachari, O. Cherifi, J. Mol. Catal. A: Chem. 260 (2006) 19–23.
- [26] K. Bachari, J.M.M. Millet, B. Benaichouba, O. Cherifi, F. Figueras, J. Catal. 221 (2004) 55–61.
- [27] V.R. Choudhary, S.K. Jana, J. Mol. Catal. A: Chem. 180 (2002) 267–276.
- [28] T. Lin, X. Zhang, R. Li, T. Bai, S.Y. Yang, Chin. Chem. Lett. 22 (2011) 639–642.
- [29] V.R. Choudhary, S.K. Jana, B.P. Kiran, Catal. Lett. 59 (1999) 217–219.
- [30] Y. Sun, S. Walspurger, J.P. Tessonnier, B. Louis, J. Sommer, Appl. Catal. A: Gen. 300 (2006) 1–7.
- [31] A. Arafat, Y. Alhamed, J. Porous. Mater. 16 (2009) 565–572.
- [32] M. Jarlbring, L. Gunneriusson, B. Hussmann, W. Forsling, J. Colloid Interf. Sci. 285 (2005) 212–217.
- [33] D. Walter, Thermochim. Acta 445 (2006) 195–199.
- [34] T.D. Nguyen, D. Mrabet, T.O. Do, J. Phys. Chem. C 112 (2008) 15226–15235.
- [35] V.R. Choudhary, S.K. Jana, A.S. Mamman, Micropor. Mesopor. Mat. 56 (2002) 65.